

A comprehensive defect study of tungsten disulfide (WS₂) as electron transport layer in perovskite solar cells by numerical simulation



K. Sobayel^a, Md. Akhtaruzzaman^{b,*}, K.S. Rahman^b, M.T. Ferdaous^a, Zeyad A. Al-Mutairi^d, Hamad F. Alharbi^d, Nabeel H. Alharthi^e, Mohammad R. Karim^e, S. Hasmady^c, N. Amin^{a,c,*}

^a Department of Electrical, Electronic and Systems Engineering, Faculty of Engineering and Built Environment, The National University of Malaysia, 43600 Bangi, Selangor, Malaysia

^b Solar Energy Research Institute, The National University of Malaysia, 43600 Bangi, Malaysia

^c Institute of Sustainable Energy, Universiti Tenaga Nasional (@The National Energy University), Jalan IKRAM-UNITEN, 43000 Kajang, Selangor, Malaysia

^d Mechanical Engineering Department, King Saud University, P.O. Box 800, Riyadh 11421, Saudi Arabia

^e Center of Excellence for Research in Engineering Materials, King Saud University, Riyadh 11421, Saudi Arabia

ARTICLE INFO

Keywords:

Perovskite solar cells
WS₂ thin films
Hole transport layers
Electron transport layer
Amphoteric defects
Interface properties
Numerical simulation
SCAPS-1D

ABSTRACT

In this study, an ideal planar perovskite solar cell (PSC) has been proposed and simulated by using Tungsten Disulfide (WS₂) as an electron transport layer (ETL). Effects of various amphoteric defect states of PSC based on CH₃NH₃PbI_{3-x}X_x absorber layer and the interface properties of both ETL and hole transport layer (HTL) are quantitatively analysed by SCAPS-1D numerical simulator. Results show that the device performance is highly influenced by amphoteric defects in the absorber layer rather than the interface defects layer (IDL). It is also revealed that the quantitative tolerable range in CH₃NH₃PbI_{3-x}X_x and IDLs are less than 10¹⁵ cm⁻³ and 10¹⁶ cm⁻³, respectively. The PSC exhibits better performance in the range of 10 °C–40 °C and degrades gradually at higher temperature. With the proposed structure, the simulation finds the highest power conversion efficiency (PCE) of PSC to be 25.70% (Voc = 1.056 V, Jsc = 25.483 mA/cm², and FF = 88.54%).

Introduction

The hybrid organic–inorganic perovskite solar cells (PSCs) based on methylammonium lead halide CH₃NH₃PbX₃ (X is Cl, Br or I) have acquired a great interest in research community due to high-power-conversion efficiency (PCEs) [1–3]. The underlying PCE of around 10% has quickly been supplanted by higher values ranging from 12% to more than 22% within a brief timeframe [4–13]. Due to continuous advancement of device architectures and material processing technologies, fabrication of PSC stands out amongst the most bracing new photovoltaic technology today. This noteworthy increment in execution, which has emphatically empowered numerous exploratory and hypothetical examinations, brings the end goal to upgrade the outline of the structure and the choice of materials. Several works are aimed for focusing on the innovative execution that guarantees to accomplish high PCEs at lower cost and flexibility [1,14,15].

In assessment to the fast development in device efficiency, the basic understanding regarding the defect properties that play a major role in

general device performance remains restrained. It is delicate to say that a semiconductor such as perovskite having doped by its own crystalline will encounter defects [16,17]. In particular, defects inside the band gap with deep transition can entice carriers, which results into Shockley–Read–Hall non-radiative recombination centres. Thus, the investigation of the defect properties in halide perovskite photovoltaics is needs to steer for further improvement of the potency. It is already reported that the defect energy distribution in the CH₃NH₃PbI₃ layer in PSC has a deep defect state of 0.16 eV above the valence band. As per hypothetical calculations, the defect state is potentially ascribed to solely low-energy deep traps [18]. It is also revealed that these defects possess non-radiative recombination centres and native type of defects in nature [19].

In PSC, a few hundred nanometre-thick perovskite absorber layer is sandwiched between an electron transport layer (ETL) and hole transport layer (HTL). This absorber layer can be with or without mesoporous scaffold. Carriers like electrons and holes, are created after the absorption of light. Thus, being excited by incident photon, carriers

* Corresponding authors at: Solar Energy Research Institute, Universiti Kebangsaan Malaysia (@The National University of Malaysia), Selangor, Malaysia (Md. Akhtaruzzaman). Institute of Sustainable Energy, Universiti Tenaga Nasional (@The National Energy University), Jalan IKRAM-UNITEN, 43000 Kajang, Selangor, Malaysia (N. Amin).

E-mail addresses: akhtar@ukm.edu.my (Md. Akhtaruzzaman), nowshad@uniten.edu.my (N. Amin).

<https://doi.org/10.1016/j.rinp.2018.12.049>

Received 4 December 2018; Accepted 10 December 2018

Available online 14 December 2018

2211-3797/ © 2018 Published by Elsevier B.V. This is an open access article under the CC BY-NC-ND license (<http://creativecommons.org/licenses/by-nc-nd/4.0/>).

travel through a hauling passage. Thereby it is needless to mention that this carrier pathway, from the absorber to both electrodes, have a great impact on PCE [20,22,23]. In recent times, the incorporation of new materials in the above-mentioned pathway, especially in ETL, has drawn huge attention of the scientific community to further improve the PCE of PSC [24–30]. TiO_2 is a notable inorganic material that is commonly used as the ETL in PSCs [20]. It has an electron mobility of approximately $1 \text{ cm}^2 \text{ V}^{-1} \text{ s}^{-1}$ with conduction band minimum (CBM) of 4.2 eV [21]. The CBM of TiO_2 is moderately 0.3 eV lower than MAPbI_3 [22,23]. Due to this, it facilitates the infusion of photo-generated electrons from perovskite absorber to the ETL. It also possesses low interfacial recombination with slightly lower charge extraction attributes. However, it has moderately low electron mobility and TiO_2 -based PSCs degrade quickly once exposed to ultraviolet radiation illumination [22–24]. Furthermore, TiO_2 commonly requires high-temperature sintering of around 500°C , which expands the vitality pay-back time and limits the production of flexible solar cells [1].

Despite of the fact that the most efficient PSCs to date are having TiO_2 and ZnO based materials [25–27], some metal oxides such as SnO_2 , Nb_2O_5 , In_2O_3 and SrTiO_3 have proven potential to be photo-electrodes in dye-sensitized solar cells (DSSCs). However, they are found to be inferior in overall performance in comparison to the TiO_2 in DSSCs. This drawback widens the scope of developing new materials in respect to the understanding of PSC's performance. Recently, transition metal dichalcogenides (TMDCs), such as molybdenum disulphide (MoS_2), tungsten disulphide (WS_2) have gained significant attention in the PV community due to their unique electrical, optical and electro-chemical properties, which make them promising materials in visible-light optical devices [28,29]. These TMDCs have been applied to Copper indium gallium (di)selenide (CIGS) or Cadmium telluride (CdTe) solar cells and achieved noteworthy success [30–32]. Among the TMDCs, WS_2 exhibits high carrier mobility, good conductivity in the order of $10^{-3} \Omega^{-1} \text{ cm}^{-1}$ and native n-type semiconducting characteristics [34,41]. Li et al. reported that WS_2 exhibits excellent electron conduction property in dye synthesized solar cell. Moreover, it can be deposited through a solution process or by sputtering at low temperature [32,33–35]. In the recent past some researchers have successfully fabricated TMDC in organic solar cell devices, including bulk-heterojunction, organic-inorganic quantum dot solar cells and perovskite solar cells. It is already reported that layered MoS_2 has been used as the hole-transport layer (HTL), electron-transport layer (ETL), interfacial layer, and protective layer in fabricating heterojunction solar cells. [56–58] Therefore, a highly stable, non-toxic and environmentally friendly n-type semiconductor makes WS_2 a potential candidate as the ETL in PSC.

In this study, we have proposed to evaluate WS_2 as a possible alternative for TiO_2 in planar perovskite solar cells. The key parameters of the PSC with the configuration of $\text{FTO}/\text{WS}_2/\text{CH}_3\text{NH}_3\text{PbI}_{3-x}\text{Cl}_x/2,2',7,7'$ -tetrakis (N, N'-di-p-methoxyphenyl amine)-9,9-spirobifluorene (Spiro-OMeTAD)/Ni have been optimized by numerical computation using SCAPS-1D simulation programme. Amphoteric defects in $\text{CH}_3\text{NH}_3\text{PbI}_{3-x}\text{Cl}_x$ absorber layer and both of its interface properties ($\text{WS}_2/\text{CH}_3\text{NH}_3\text{PbI}_{3-x}\text{Cl}_x$ and $\text{CH}_3\text{NH}_3\text{PbI}_{3-x}\text{Cl}_x/\text{Spiro-OMeTAD}$) are thoroughly investigated in order to understand their effects on the PSC's performance.

Simulation setup and parameter

SCAPS-1D program (version 3.3.05) [38] has been commonly used for numerical simulations of a solar cell devices [39,40]. Many previous studies [33,35,41,45] have utilized SCAPS software to display planar structure of PSC (p-i-n) because of their structural similarity with other types of solar cells. This simulation program numerically solves three essential semiconductor equations: The Poisson equation and the continuity equation for holes and the continuity equation for electrons. In this study, an escalated hypothetical numerical investigation has been

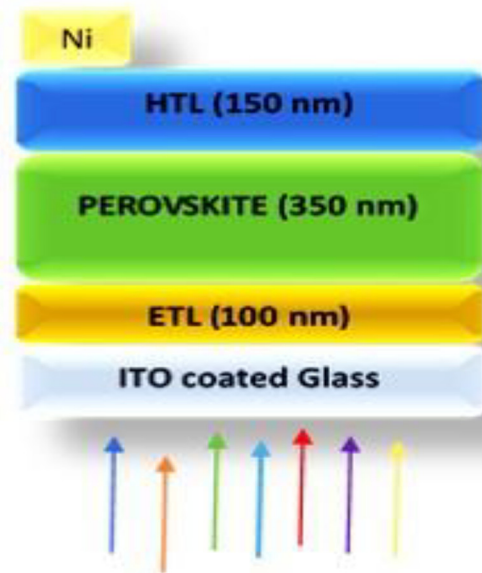


Fig. 1. A schematic structure of a Perovskite Solar Cell.

performed to outline ideal ETL instead of TiO_2 and to explore solar cell device mechanism for potency and device stability in ambient conditions. The examined device structure of this study is shown in

Fig. 1.

In this work, intrinsic perovskite is used as an absorber layer with the proposition of n-i-p planar PSC structure. This model has been simulated with basic three input layers; p-type Spiro-OMeTAD is used as HTL, intrinsic perovskite ($\text{CH}_3\text{NH}_3\text{PbI}_{3-x}\text{Cl}_x$) as absorber layer and n-type WS_2 as ETL. Hence solar energy is considered to enter through the ETL layer. A standard AM1.5G spectrum (1000 W/m^2 ; $T = 300 \text{ K}$) has been used for illumination. Typical thicknesses of each layer were fixed. In particular, 350 nm thick perovskite absorber layer is considered as it ensures a radiation absorption close to the maximum, without major recombination losses [36–38]. For initial consideration, ETL and HTL thickness are set to be 100 nm and 150 nm respectively [41,46,47]. Interface defect layers (IDL) of 10 nm thickness were used in the perovskite/ETL interface to determine the effect of defect densities that subsist at material interfaces. Moreover, to replicate the defects of PSC, amphoteric native defect model is used in simulation where the density of defect in active layer was varied. Fig. 2 demonstrates the band alignment of the proposed model and Table 1 summarizes the physical parameters used for each layer in the numerical analysis. All the

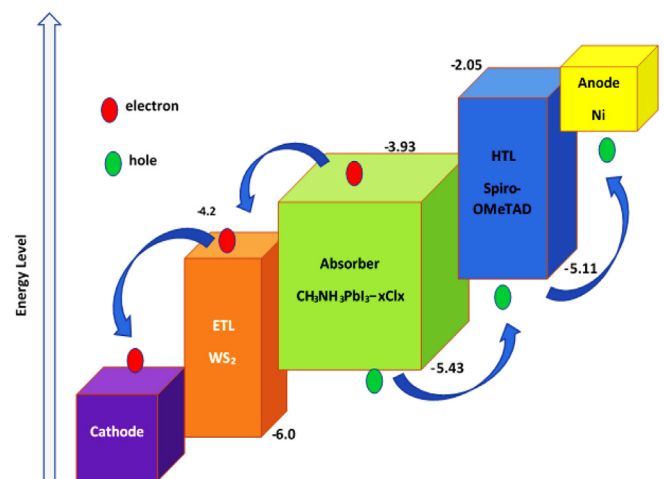


Fig. 2. Band alignment of proposed PSC structure.

Table 1
Parameters used for simulation study.

Parameters	CH ₃ NH ₃ PbI ₃	IDL (Perovskite /ETL interface)	WS ₂	Spiro-OMeTAD
Thickness (nm)	350	10	100	150
E _g (eV)	1.55	1.55	1.8	3.06
χ (eV)	3.93	3.9	3.95	2.05
ε _r	18	18	13.6	3
μ _e (cm ² /Vs)	3	3	100	2.0 × 10 ⁻⁴
μ _h (cm ² /Vs)	17	17	100	2.0 × 10 ⁻⁴
N _D (cm ⁻³)	2.0 × 10 ¹⁰	2.0 × 10 ¹⁰	1.0 × 10 ¹⁸	–
N _A (cm ⁻³)	2.0 × 10 ¹⁰	–	–	1.0 × 10 ¹⁸
N _t (cm ⁻³)	1.0 × 10 ¹⁰	1.0 × 10 ¹⁵	1.0 × 10 ¹⁵	1.0 × 10 ¹⁵

parameters used in this study are supported by various literature [35,39–44,46,47].

Despite of the parameters depicted in the Table 1, following values are considered irrespective of type of layers: thermal velocity of electrons and holes of 1×10^7 cm/s; Gaussian defect distribution all defect states, ETL and HTL interfaces defects are at the middle of interface gap and characteristic energy of 0.1 eV.

Results and discussion

Baseline WS₂/CH₃NH₃PbX₃/Spiro-OMeTAD solar cell devices

Initial simulation has been conducted using device geometry as cathode/WS₂/CH₃NH₃PbX₃/Spiro-OMeTAD/ Ni depicted in Fig. 1. As there is no reported experimental work on WS₂ as buffer layer, CH₃NH₃PbX₃ based device in the n-i-p configuration with TiO₂ and Spiro-OMeTAD as

ETL and HTL respectively; has been taken into consideration for comparison between simulated J-V and QE curves shown in Fig. 3(a) and (b) with experimental results [48]. The discrepancy in J_{sc} is likely because of different buffer layer material and non-consideration of refractive indexes of layers by SCAPS 1D. SCAPS 1D underestimates QE within the longer wavelength spectral region where light moves for the second pass to complete absorption, and so, a higher limit of optical J_{sc} is conferred. Dielectric function spectra of all the layers are also considered by optical simulation and thus, multiple reflections at various interfaces play a big role in QE. As comparison is done between two different materials, there exists differences between their refractive and reflective indexes which leads to the result of different QE of studied device. Most importantly, the proposed FTO/WS₂/CH₃NH₃PbI_{3-x}Cl_x/Spiro-OMeTAD/Ni device shows the efficiency of 25.70% with J_{sc} of 25.48 mA/cm², fill factor of 88.84% and Voc of 1.05 V in SCAPS-1D.

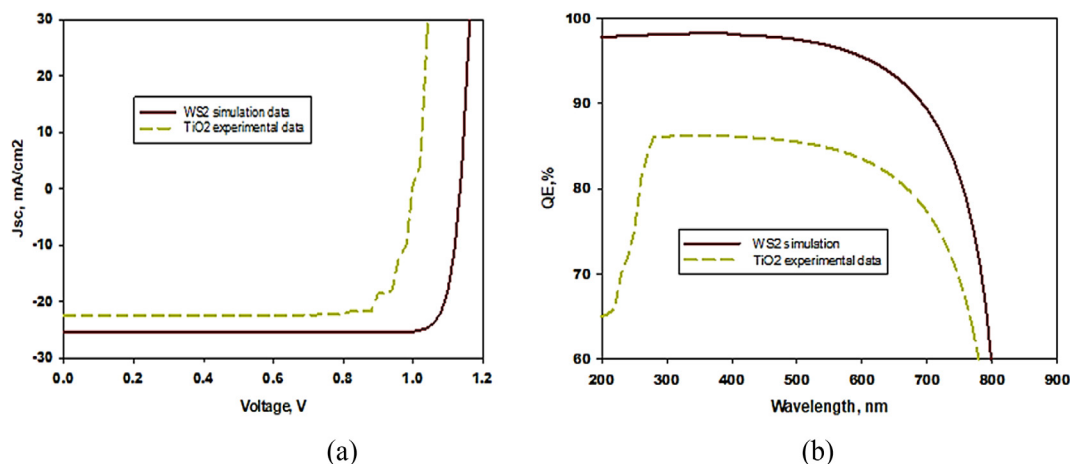


Fig. 3. (a) J-V curves and (b) QE curves obtained from SCAPS 1D simulation as compared with an experimental data [48] for a n-i-p perovskite device.

Being a baseline simulation study, no defect is considered in this simulation.

Effects of the amphoteric defect state in MAPbX₃

In perovskite CH₃NH₃Pb-X₃ (X = Cl, Br, I) layer, CH₃NH₃ and Pb provide one and two electrons, respectively, to three halide (X) particles, forming a bandgap of 1.5 eV. In forming Pb-X₂, the CH₃NH₃ molecule does not have any significant commitment but to donate an electron. Interestingly, CH₃NH₃Pb-X₃ layer exhibits different types of conductivity, intrinsic good p-type, moderate n-type, based on deposition properties of Pb and halide molecules. Such flexible characteristic of CH₃NH₃Pb-X₃ lead to defect such as their native defect or other various interface defects [49–51]. Defect properties in absorber layer of solar cell play a critical role to determine the electron-hole diffusion length and open circuit voltage, (Voc). Deep level defects usually act as Shockley-Read-Hall non-radiative recombination centres. It is proved that these types of defects are responsible for short minority carrier lifetime which results into lower Voc in solar cell. Again, if the defect state reaches up to the transition level for instance, at Fermi level position, then this can also act as Shockley-Read-Hall nonradiative recombination centres by donating/accepting electrons in the bandgap. Initially the idea of amphoteric defects was acquainted with clarifying impacts of native (or inherent) defects on the properties of semiconducting materials including the sticking of the Fermi level energy on semiconductor surfaces, stabilization of the Fermi energy in vigorously defective semiconductors arrangement of Schottky boundaries and drawbacks of doping of semiconductors. More recently the concept of amphoteric native defects has been used to control defect incorporation in compound semiconductors like CH₃NH₃Pb-X₃ in PSC devices [52].

Fig. 4 shows the effects of amphoteric defect states to MAPbI₃. Both the efficiency and Voc varies with the density of defect states in MAPbI₃. From the Fig. 4(a), it can be seen that when the density of defect states in MAPbI₃ increases from 13th order to higher value, the Voc reduces significantly and causes drop of efficiency (less than 10%). In addition, when the density of defect states is lower than 1×10^{15} cm⁻³, the Voc remains above about 0.8 V and efficiency shows above 15% on that range. Moreover, if the density of the defect state is larger than 1×10^{15} cm⁻³, the Voc decreases to about 0.5 V which is impractical for solar cell application. Fig. 4(b) depicts the change of J_{sc} versus the density of defects in MAPbI₃ with respect to the efficiency of a cell. The figure shows a clear impact of amphoteric defect on J_{sc} and efficiency. J_{sc} changes from 25.4 to 20.8 mA/cm² with the change of density of the defect state from 1×10^{10} to 1×10^{13} cm⁻³. In this range, cell efficiency drops very little, only by 4.6%. Efficiency drops significantly when density of the defect state is higher than

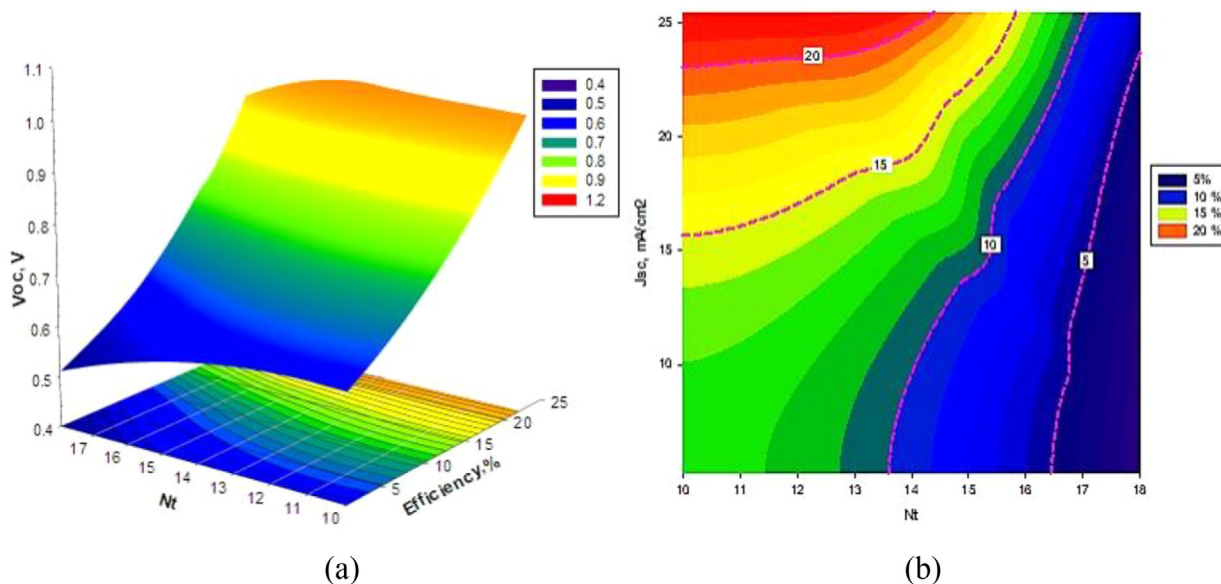


Fig. 4. Effects of the change of (a) Efficiency and Voc versus the amphoteric defect density N_t and (b) J_{sc} and efficiency versus the amphoteric defect density in $CH_3NH_3Pb-X_3$ (MAPb- X_3).

$1 \times 10^{14} \text{ cm}^{-3}$, the J_{sc} and efficiency falls sharply with the increment of amphoteric defect state from $1 \times 10^{16} \text{ cm}^{-3}$.

Effects of defect states in IDL1

Effects of defect states in both the interfaces of PSC, IDL1 ($WS_2/$ MAPbI₃) and IDL2 (MPbI₃/Spiro-OMeTAD), have been studied in detail. Figs. 5 and 6 represent the defect study in IDL1 and IDL2, respectively. It clearly shows that the cell efficiency drops drastically when defect density of IDL1 is $1 \times 10^{18} \text{ cm}^{-3}$ or more. Moreover, it is revealed that there is slight change of efficiency with the range of IDL1 defect state $1 \times 10^{15} \sim 1 \times 10^{17} \text{ cm}^{-3}$. But in case of Voc, it has been observed that the Voc drops from 0.85 V to 0.68 V when defect density increases from $1 \times 10^{16} \text{ cm}^{-3}$ or higher values. There is hardly any change of Voc beyond $1 \times 10^{16} \text{ cm}^{-3}$ of defect density in IDL1.

Effects of defect states in IDL2

Almost the same results depict for IDL2 as shown in Fig. 6. It has been examined that the cell efficiency goes significantly downward, 22% to 12%, when defect density at IDL2 is increased from $1 \times 10^{17} \text{ cm}^{-3}$ or more. In the range of defect state density $1 \times 10^{14} - 1 \times 10^{16} \text{ cm}^{-3}$ in IDL2, device efficiency changes a little (25.4%–21.31%). In the case of Voc, it has been observed that Voc drops from 1.1 V to 0.697 V when defect density is $1 \times 10^{15} \text{ cm}^{-3}$ or more. It is also found (Fig. 6b) that defect plays a cogent role when it is near to the MPbI₃/Spiro-OMeTAD interface, 0.1 eV–0.4 eV, Voc and efficiency are also found to be lesser in this condition. But if the defect state is far from the interface (above 0.9 eV); it has a very limited impact both in Voc and efficiency of the PSC. It is examined that fill factor of PSC is highly affected by the increment of defect; when the density of the defect state in IDL2 achieves the value of $1 \times 10^{16} \text{ cm}^{-3}$ or more, the FF decreases (Fig. 6C) from 87% to around 81%. The simulation also

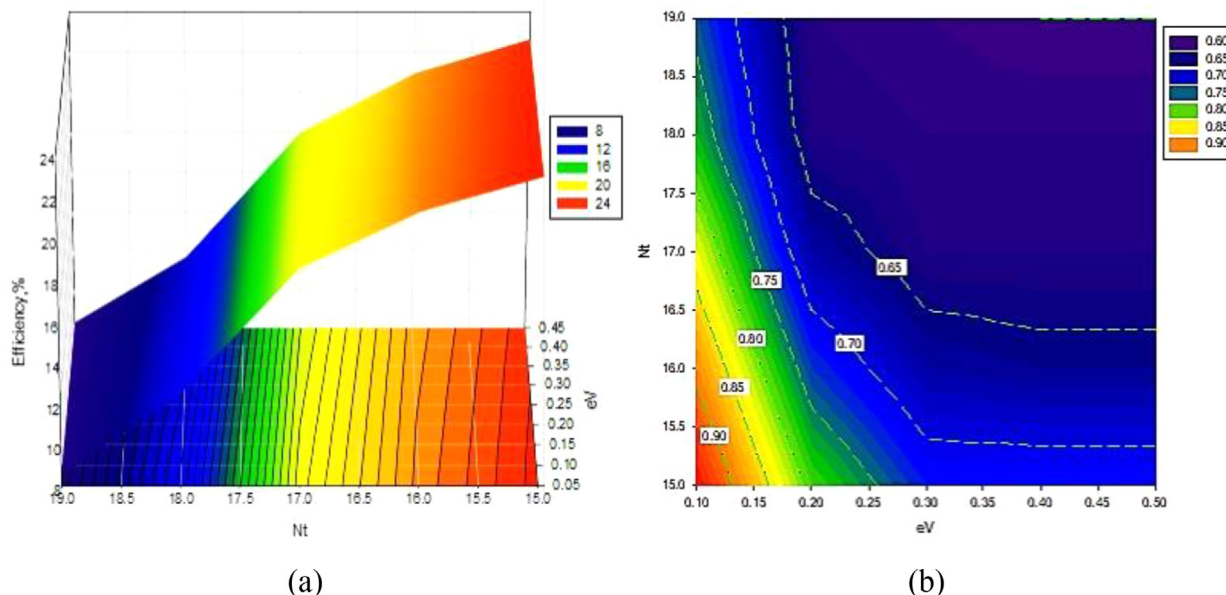


Fig. 5. Effect of the change of (a) Efficiency with defect density and (b) Voc with respect to defect position versus various defect density in IDL1 of MAPbI₃.

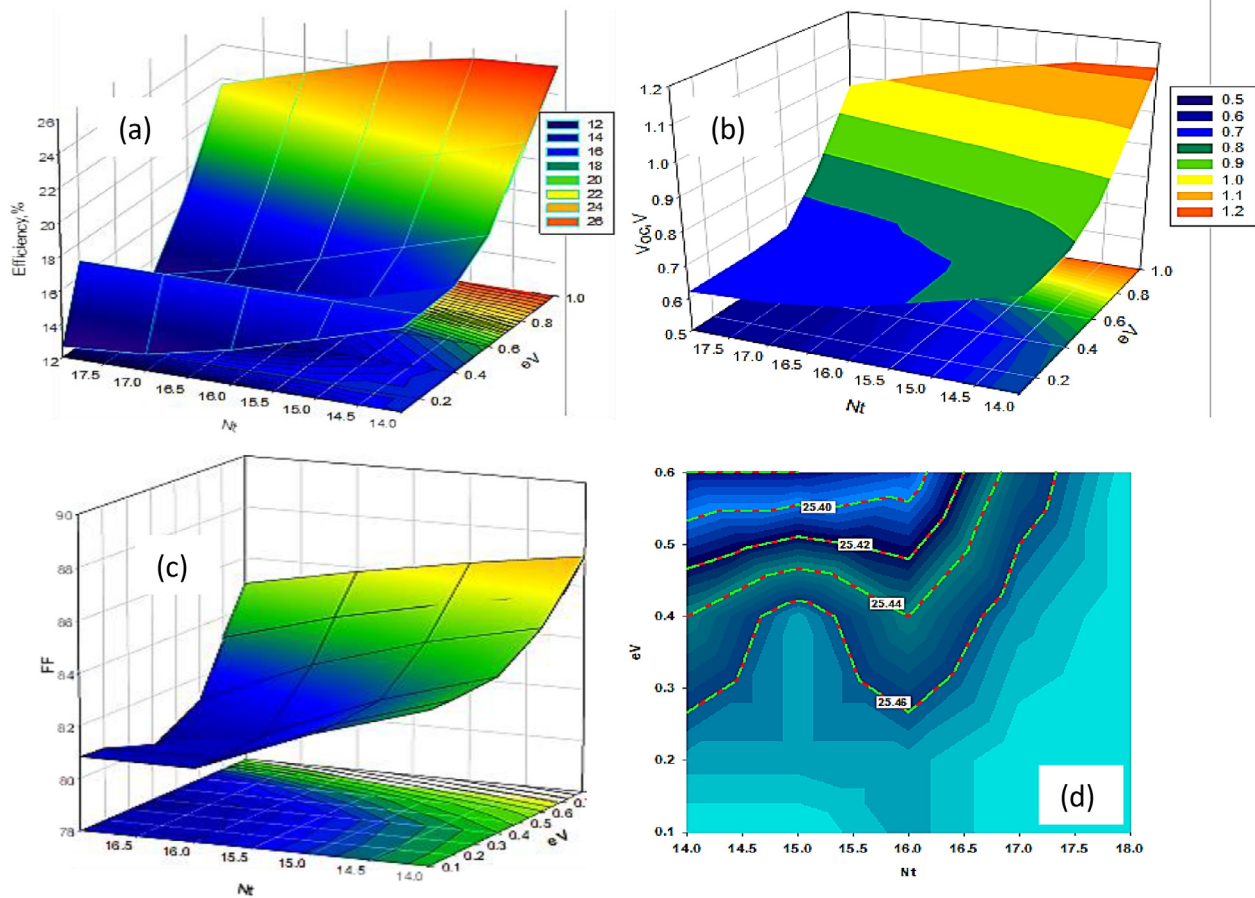


Fig. 6. Effect of the change of (a) Efficiency with the defect density and (b) Voc with respect to defect position versus various defect density (c) fill factor and (d) Jsc with the density of defect in IDL2 of MAPbI₃.

shows that density of defect has very less impact on Jsc (Fig. 6d).

Effects of temperature on PSC

Solar cells are generally installed in the outdoor environment. Thus, sunlight falls on it directly and causes increment in temperature, even by 45 °C higher than environmental temperature. For example, if the environmental temperature is 30 °C, the device temperature can rise up to 75 °C [54]. From various experiment on PSC, it showed that the most challenging concern for PSC is long-term stability [53,55]. The main reason for degradation is decrement in the shunt resistance which results lowering of both Voc and Fill Factor [54]. Researchers found that in high temperature and humid atmosphere, CH₃NH₃PbI₃ could be corroded by 4-*tert*-butylpyridine (4-tBP) and may also change the phase, which causes degradation of PSC performance [53].

Fig. 7 shows the effect of working temperature on the performance of PSC solar cell by changing environmental temperature from 10 °C to 90 °C. It is found (Fig. 7a) that both Voc and FF are badly affected by the higher temperature, which confirms to experimental study done by Han et al. [55]. But there are hardly any changes that can be observed in Jsc. As higher temperature affects both Voc and FF, the efficiency eventually reduces. As shown in Fig. 7b, this study confirms that PSC at ambient atmosphere (10 °C to 40 °C) provides higher efficiency, which is above 23%; but gradually decreases as the temperature rises. This finding can play a crucial role in selecting PSC in tropical regions.

Conclusion

In an attempt to enhance device stability, improve performance and

curtail hysteresis behaviour in PSCs, the possibility of WS₂ as an alternative ETL material has been investigated for the first time by SCAPS-1D simulator. The numerical simulation mainly addresses the issues related to amphoteric defects and temperature. Results revealed that theoretically WS₂ can replace the TiO₂ as ETL in PSC, whereby amphoteric defect states have a great influenced on the efficiency of PSC when the density of defect state is higher than 10¹⁵ cm⁻³. It has also been found that buffer/absorber interface and absorber/HTL interface defects play a major role when the density of defect state is higher than 10¹⁷ cm⁻³ and 10¹⁶ cm⁻³, respectively. Finally, PSC demonstrates better performance when working temperature is in the range of 10 °C–40 °C. The optimized structure with a PCE of 25.70% (Voc = 1.321 V, Jsc = 25.483 mA/cm² and FF = 88.54%) certainly enlightens the possibility of WS₂ as a potential ETL. This investigation opens up the pathway for reasonable usage of any TMDCs, especially WS₂ as the prospective ETL for PSCs.

Acknowledgement

The authors would like to acknowledge the contribution of The National University of Malaysia through the research grant with code GUP-2018-130. Due appreciation is also credited to the Institute of Sustainable Energy (ISE) of the Universiti Tenaga Nasional (@The National Energy University) of Malaysia for their cordial support through BOLD2025 Program. The authors gratefully acknowledge to Dr. Marc Bargeman, University of Gent, Belgium, for providing the SCAPS simulation software.

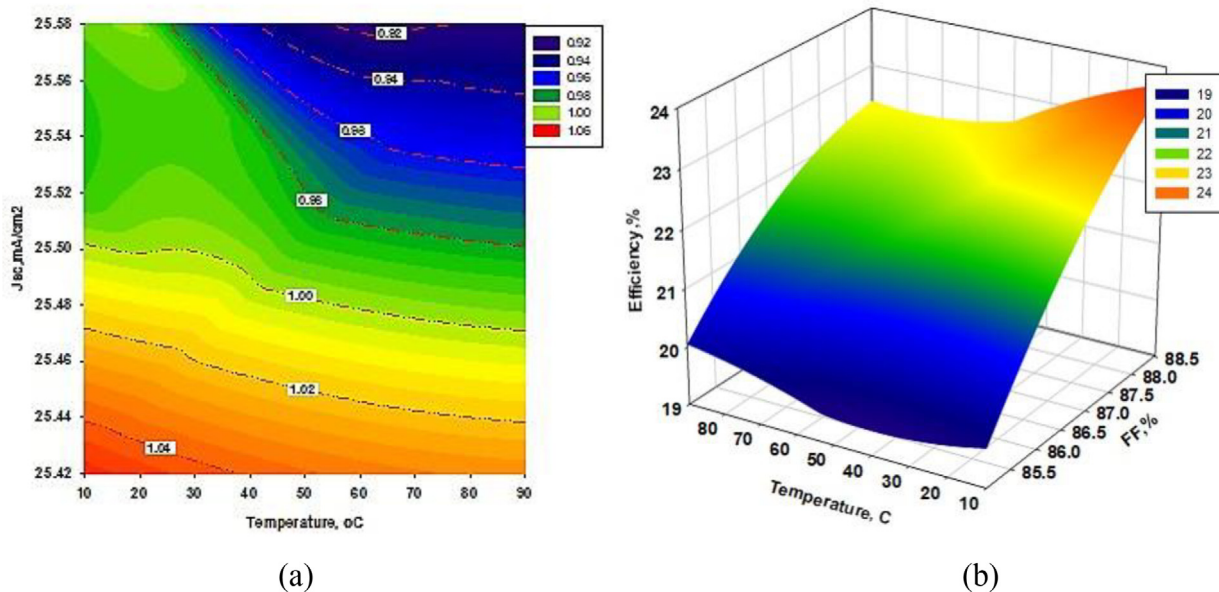


Fig. 7. Effect of environmental temperature with respect to (a) J_{sc} and V_{oc} ; (b) efficiency and fill factor of MAPbI_3 .

Appendix A. Supplementary data

Supplementary data to this article can be found online at <https://doi.org/10.1016/j.rinp.2018.12.049>.

References

- [1] Green MA, Ho-Baillie A, Snaith HJ. The emergence of perovskite solar cells. *Nat Photon* 2014;8(7): pp. nphoton-2014.
- [2] Snaith HJ. Perovskites: the emergence of a new era for low-cost, high-efficiency solar cells. *J Phys Chem Lett* 2013;4(21):3623–30.
- [3] Kim HS, Im SH, Park NG. Organolead halide perovskite: new horizons in solar cell research. *J Phys Chem C* 2014;118(11):5615–25.
- [4] Noh JH, Im SH, Heo JH, Mandal TN, Seok SI. Chemical management for colorful, efficient, and stable inorganic–organic hybrid nanostructured solar cells. *Nano Lett* 2013;13(4):1764–9.
- [5] Burschka J, Pellet N, Moon SJ, Humphry-Baker R, Gao P, Nazeeruddin MK, et al. Sequential deposition as a route to high-performance perovskite-sensitized solar cells. *Nature* 2013;499(7458):316–9.
- [6] Chen Q, Zhou H, Hong Z, Luo S, Duan HS, Wang HH, et al. Planar heterojunction perovskite solar cells via vapor-assisted solution process. *J Am Chem Soc* 2013;136(2):622–5.
- [7] Kim HS, Lee CR, Im JH, Lee KB, Moehl T, Marchioro A, et al. Lead iodide perovskite sensitized all-solid-state submicron thin film mesoscopic solar cell with efficiency exceeding 9%. *Sci Rep* 2012;2:591.
- [8] Liu M, Johnston MB, Snaith HJ. Efficient planar heterojunction perovskite solar cells by vapor deposition. *Nature* 2013;501(7467):395–8.
- [9] Heo JH, Im SH, Noh JH, Mandal TN, Lim CS, Chang JA, et al. Efficient inorganic–organic hybrid heterojunction solar cells containing perovskite compound and polymeric hole conductors. *Nat Photon* 2013;7(6):486.
- [10] Liu D, Kelly TL. Perovskite solar cells with a planar heterojunction structure prepared using room-temperature solution processing techniques. *Nat Photon* 2014;8(2):133.
- [11] Zhang W, Saliba M, Stranks SD, Sun Y, Shi X, Wiesner U, et al. Enhancement of perovskite-based solar cells employing core–shell metal nanoparticles. *Nano Lett* 2013;13(9):4505–10.
- [12] Ball JM, Lee MM, Hey A, Snaith HJ. Low-temperature processed meso-structured to thin-film perovskite solar cells. *Energy Environ Sci* 2013;6(6):1739–43.
- [13] Lee MM, Teuscher J, Miyasaka T, Murakami TN, Snaith HJ. Efficient hybrid solar cells based on meso-superstructure organometal halide perovskites. *Science* 2012;1228604.
- [14] Park NG. Organometal perovskite light absorbers toward a 20% efficiency low-cost solid-state mesoscopic solar cell. *J Phys Chem Lett* 2013;4(15):2423–9.
- [15] Zuo C, Bolink HJ, Han H, Huang J, Cahen D, Ding L. Advances in perovskite solar cells. *Adv Sci* 2016;3(7):1500324.
- [16] Yin WJ, Shi T, Yan Y. Unique properties of halide perovskites as possible origins of the superior solar cell performance. *Adv Mater* 2014;26(27):4653–8.
- [17] Kim J, Lee SH, Lee JH, Hong KH. The role of intrinsic defects in methylammonium lead iodide perovskite. *J Phys Chem Lett* 2014;5(8):1312–7.
- [18] Duan HS, Zhou H, Chen Q, Sun P, Luo S, Song TB, et al. The identification and characterization of defect states in hybrid organic–inorganic perovskite photovoltaics. *PCCP* 2015;17(1):112–6.
- [19] Du MH. Efficient carrier transport in halide perovskites: theoretical perspectives. *J Mater Chem A* 2014;2(24):9091–8.
- [20] Yang G, Tao H, Qin P, Ke W, Fang G. Recent progress in electron transport layers for efficient perovskite solar cells. *J Mater Chem A* 2016;4(11):3970–90.
- [21] Tiwana P, Docampo P, Johnston MB, Snaith HJ, Herz LM. Electron mobility and injection dynamics in mesoporous ZnO , SnO_2 , and TiO_2 films used in dye-sensitized solar cells. *ACS Nano* 2011;5(6):5158–66.
- [22] Geng W, Tong CJ, Liu J, Zhu W, Lau WM, Liu LM. Structures and electronic properties of different $\text{CH}_3\text{NH}_3\text{PbI}_3/\text{TiO}_2$ interface: a first-principles study. *Sci Rep* 2016;6:20131.
- [23] Liu C, Wang K, Yi C, Shi X, Du P, Smith AW, et al. Ultrasensitive solution-processed perovskite hybrid photodetectors. *J Mater Chem C* 2015;3(26):6600–6.
- [24] Leijtens T, Eperon GE, Pathak S, Abate A, Lee MM, Snaith HJ. Overcoming ultraviolet light instability of sensitized TiO_2 with meso-superstructure organometal tri-halide perovskite solar cells. *Nat Commun* 2013;4:2885.
- [25] Eperon GE, Burlakov VM, Docampo P, Goriely A, Snaith HJ. Morphological control for high performance, solution-processed planar heterojunction perovskite solar cells. *Adv Funct Mater* 2014;24(1):151–7.
- [26] Liu D, Kelly TL. Perovskite solar cells with a planar heterojunction structure prepared using room-temperature solution processing techniques. *Nat Photon* 2014;8(2):133.
- [27] Liu M, Johnston MB, Snaith HJ. Efficient planar heterojunction perovskite solar cells by vapour deposition. *Nature* 2013;501(7467):395–8.
- [28] Dasgupta U, Chatterjee S, Pal AJ. Thin-film formation of 2D MoS_2 and its application as a hole-transport layer in planar perovskite solar cells. *Sol Energy Mater Sol Cells* 2017;172:353–60.
- [29] Huang P, Wang Z, Liu Y, Zhang K, Yuan L, Zhou Y, et al. Water-soluble 2D transition metal dichalcogenides as the hole-transport layer for highly efficient and stable p–i–n perovskite solar cells. *ACS Appl Mater Interfaces* 2017;9(30):25323–31.
- [30] Liu J, Zhuang D, Luan H, Cao M, Xie M, Li X. Preparation of $\text{Cu}(\text{In}, \text{Ga})\text{Se}_2$ thin film by sputtering from $\text{Cu}(\text{In}, \text{Ga})\text{Se}_2$ quaternary target. *Prog Nat Sci Mater Int* 2013;23(2):133–8.
- [31] Liu J, Zhuang DM, Cao MJ, Li XL, Xie M, Xu DW. $\text{Cu}(\text{In}, \text{Ga})\text{Se}_2$ -based solar cells prepared from Se-containing precursors. *Vacuum* 2014;102:26–30.
- [32] Li S, Chen Z, Zhang W. Dye-sensitized solar cells based on WS_2 counter electrodes. *Mater Lett* 2012;72:22–4.
- [33] Gourmelon E, Lignier O, Hadouda H, Couturier G, Bernede JC, Tedd J, et al. MS_2 ($M = \text{W}, \text{Mo}$) photosensitive thin films for solar cells. *Sol Energy Mater Sol Cells* 1997;46(2):115–21.
- [34] Hankare PP, Manikshete AH, Sathe DJ, Chate PA, Patil AA, Garadkar KM. WS_2 thin films: Opto-electronic characterization. *J Alloy Compd* 2009;479(1–2):657–60.
- [35] Lignier O, Couturier G, Tedd J, Gonbeau D, Salardenne J. Photoactivity enhancement of WS_2 sputtered thin films by use of nickel. *Thin Solid Films* 1997;299(1–2):45–52.
- [36] Liu F, Zhu J, Wei J, Li Y, Lv M, Yang S, et al. Numerical simulation: toward the design of high-efficiency planar perovskite solar cells. *Appl Phys Lett* 2014;104(25):253508.
- [37] Peng L et al., Device simulation of solid-state perovskite solar cells, 31st European Photovoltaic Solar Energy Conference and Exhibition; 2015.
- [38] Baktash A, Amiri O, Sasani A. Improve efficiency of perovskite solar cells by using magnesium doped ZnO and TiO_2 compact layers. *Superlattices Microstruct* 2016;93:128–37.
- [39] Adhikari KR, Gurung S, Bhattarai BK, Soucase BM. Comparative study on MAPbI_3

- based solar cells using different electron transporting materials. *Phys Stat Sol (c)* 2016;13(1):13–7.
- [40] Casas GA, Cappelletti MA, Cédola AP, Soucase BM, y Blancá EP. Analysis of the power conversion efficiency of perovskite solar cells with different materials as Hole-Transport Layer by numerical simulations. *Superlattice Microstruct* 2017;107:136–43.
- [41] Sobayel K, Rahman K, Karim M, Aijaz M, Dar MA, Shar M, et al. Numerical modeling on prospective buffer layers for tungsten DI-sulfide (WS₂) solar cells by SCAPS-1D. *Chalcogenide Lett* 2018;15(6):307–15.
- [42] Burgelman M, Nollet P, Degraeve S. Modelling polycrystalline semiconductor solar cells. *Thin Solid Films* 2000;361:527–32.
- [43] Zhou H, Chen Q, Li G, Luo S, Song TB, Duan HS, et al. Interface engineering of highly efficient perovskite solar cells. *Science* 2014;345(6196):542–6.
- [44] Cahen D, Edri E, Hodes G, Gartsman K, Kirmayer S, Mukhopadhyay S. Elucidating the charge carrier separation and working mechanism of CH₃NH₃PbI_{3-x}Cl_x perovskite solar cells. *Nat Commun* 2014;5:3461.
- [45] Minemoto T, Murata M. Device modeling of perovskite solar cells based on structural similarity with thin film inorganic semiconductor solar cells. *J Appl Phys* 2014;116(5). 054505.
- [46] Chowdhury TH, Ferdaous MT, Wadi MAA, Chelvanathan P, Amin N, Islam A, et al. Prospects of ternary Cd_{1-x}Zn_xS as an electron transport layer and associated interface defects in a planar lead halide perovskite solar cell via numerical simulation. *J Electron Mater* 2018;47(5):3051–8.
- [47] Paul S, Grover S, Repins IL, Keyes BM, Contreras MA, Ramanathan K, et al. Analysis of back-contact interface recombination in thin-film solar cells. *IEEE J Photovolt* 2018;8(3):871–8.
- [48] Niemegeers A, Burgelman M. Numerical modelling of ac-characteristics of CdTe and CIS solar cells. In: *Photovoltaic Specialists Conference, 1996, Conference Record of the Twenty Fifth IEEE*; 1996, May p. 901–904. IEEE.
- [49] Yin WJ, Shi T, Yan Y. Unusual defect physics in CH₃NH₃PbI₃ perovskite solar cell absorber. *Appl Phys Lett* 2014;104(6). 063903.
- [50] Walukiewicz W. Mechanism of Schottky barrier formation: the role of amphoteric native defects. *J Vacu Sci Technol B: Microelectron Process Phenom* 1987;5(4):1062–7.
- [51] Walukiewicz W. Fermi level dependent native defect formation: consequences for metal–semiconductor and semiconductor–semiconductor interfaces. *J Vacu Sci Technol B: Microelectron Process Phenom* 1988;6(4):1257–62.
- [52] Alberi K, Scarpulla MA. Suppression of compensating native defect formation during semiconductor processing via excess carriers. *Sci Rep* 2016;6:27954.
- [53] Leijtens T, Eperon GE, Pathak S, Abate A, Lee MM, Snaith HJ. Overcoming ultra-violet light instability of sensitized TiO₂ with meso-superstructure organometal tri-halide perovskite solar cells. *Nat Commun* 2013;4:2885.
- [54] Cuddihy E, Coulbert C, Gupta A, Liang R. Electricity from photovoltaic solar cells: flat-plate solar array project final report. Volume VII: Module encapsulation; 1986.
- [55] Han Y, Meyer S, Dkhissi Y, Weber K, Pringle JM, Bach U, et al. Degradation observations of encapsulated planar CH₃NH₃PbI₃ perovskite solar cells at high temperatures and humidity. *J Mater Chem A* 2015;3(15):8139–47.
- [56] Yun J, Noh Y, Yeo J, Go Y, Na S, Jeong H, et al. Efficient work-function engineering of solution-processed MoS₂ thin-films for novel hole and electron transport layers leading to high-performance polymer solar cells. *J Mater Chem C* 2013;1:3777–83.
- [57] Singh E, Kim KS, Yeom GY, Nalwa HS. Atomically thin-layered molybdenum disulfide (MoS₂) for bulk-heterojunction solar cells. *ACS Appl Mater Interf* 2017;9(4):3223–45. <https://doi.org/10.1021/acsami.6b13582>.
- [58] Singh E, Kim KS, Yeom GY, Nalwa HS. Two-dimensional transition metal dichalcogenide-based counter electrodes for dye-sensitized solar cells. *RSC Adv* 2017;7(45):28234–90.